Reinforcement Learning informs optimal treatment strategies to limit antibiotic resistance.

Davis T. Weaver[1,2], **Jeff Maltas**[2,†], **and Jacob G. Scott**[1,2,3,†]

[1]Case Western Reserve University School of Medicine, Cleveland, OH, 44106, USA
[2]Translational Hematology Oncology Research, Cleveland Clinic, Cleveland OH, 44106, USA
[3]Department of Physics, Case Western Reserve University, Cleveland, OH, 44106, USA
[†]jeff.maltas@gmail.com, scottj10@ccf.org

ABSTRACT

Drug resistant pathogens are a wide-spread and deadly phenomenon. Antimicrobial resistance was estimated to be associated with 4.95 million deaths worldwide in 2019. If resistance continues to develop at the current rate, bacterial infections are expected to surpass cancer as the leading cause of death worldwide by 2050. Despite this troubling trend, antimicrobial drug development has all but ceased. For the few new drugs that are approved, microbes develop rapid resistance through evolution by mutation and selection. Novel approaches to designing therapy that explicitly take into account the adaptive nature of microbial cell populations are desperately needed. Approaches that can design therapies given limited information about the evolving system are particularly important due to the limitations of clinical measurement. In this study, we explore a reinforcement learning (RL) approach capable of learning effective drug cycling policies in a system defined by empirically measured fitness landscapes. Given access to a panel of 15 β-lactam antibiotics with which to treat the simulated *E. Coli* population, we demonstrate that RL agents outperform two potential treatment paradigms at minimizing the population fitness over time. We also show that RL agents approach the performance of the optimal drug cycling policy. Crucially, we show that it is possible for RL agents to learn effective drug cycling protocols using current population fitness as the only training input. Our work represents a proof-of-concept for using AI to control complex evolutionary processes.

Conflict of Interest Statement: The authors have no conflicts of interest to disclose.

Introduction

Drug resistant pathogens are a wide-spread and deadly phenomenon that were responsible for nearly 5 million deaths worldwide in 2019[1]. In the US alone, 3 million cases of antimicrobial resistant infections are observed each year[2]. The increasing prevalence of pan-drug resistance has prompted the CDC to declare that we have entered a "post-antibiotic era"[2]. Despite this evident public health crisis, development of novel antibiotics has all but ceased due to the poor return on investment currently associated with this class of drugs[3]. Novel approaches to designing therapies that explicitly take into account the adaptive nature of microbial cell populations while leveraging existing treatment options are desperately needed.

Evolutionary medicine is a rapidly growing discipline that aims to develop treatment strategies that explicitly account for the capacity of pathogens and cancer to evolve[4–10]. Such treatment strategies, termed "evolutionary therapies", typically cycle between drugs or drug doses to take advantage of predictable patterns of disease evolution. Evolutionary therapies are typically developed by applying optimization methods to a mathematical or simulation-based model of the evolving system under study[11–21]. For example, in castrate-resistant prostate cancer, researchers developed an on-off drug cycling drug protocol that allows drug-sensitive cancer cells to regrow following a course of treatment[22,23]. Clinical trials have shown this therapy prevents the emergence of a resistant phenotype and enables superior long-term tumor control and patient survival compared to conventional strategies[22,23].

Current methods for the development of evolutionary therapies require an enormous amount of data on the evolving system. For example, many researchers have optimized treatment by using genotype-phenotype maps to define evolutionary dynamics and model the evolving cell population[15,24–32]. However, most methods for optimization of these models requires a complete understanding of the underlying system dynamics[14,15,33,34]. Such detailed knowledge is currently unobtainable in the clinical setting. Approaches that can approximate these optimal policies given only a fraction of the available information would fill a key unmet need in evolutionary medicine.

We hypothesize that reinforcement learning algorithms can develop effective drug cycling policies given only experimentally measurable information about the evolving pathogen. Reinforcement learning (RL) is a well-studied subfield of machine learning that has been successfully used in applications ranging from board games and video games to manufacturing automation[33,35–37]. Broadly, RL methods train artificial intelligence agents to select actions that maximize a reward function. Importantly, RL methods are particularly suited for optimization problems where little is known about the dynamics of the underlying system. Further, RL and related optimal control methods have been previously applied for the development of clinical optimization protocols in onocology and anesthesiology[20,38–43].

In this study, we develop of a novel approach to discovering evolutionary therapies, using a well studied set of empirical fitness landscapes as a model system. We will explore "perfect information" optimization methods such as dynamic programming in addition to RL methods that can learn policies given only limited information about a system. We show that it is possible to learn effective drug cycling treatments given extremely limited information about the evolving population, even in situations where the measurements reaching the RL agent is extremely noisy and the information content is low.

index	drug code	drug
1	AMP	Ampicillin
2	AM	Amoxicillin
3	CEC	Cefaclor
4	CTX	Cefotaxime
5	ZOX	Ceftizoxime
6	CXM	Cefuroxime
7	CRO	Ceftriaxone
8	AMC	Amoxicillin + Clavulanic acid
9	CAZ	Ceftazidime
10	CTT	Cefotetan
11	SAM	Ampicillin + Sulbactam
12	CPR	Cefprozil
13	CPD	Cefpodoxime
14	TZP	Pipercillin + Tazobactam
15	FEP	Cefepime

Table 1. Reference codes for drugs under study

1 Methods

As a model system, we simulated an evolving population of *Escherichia coli (E. coli)* using the well-studied fitness landscape paradigm, where each genotype is associated with a certain fitness under selection[15,25,28]. We relied on a previously described 4 allele landscape of the *E. Coli* β-lacatamase gene where each mutation has a measured impact on the sensitivity of an *E. coli* population to one of 15 β-lactam antibiotics[25,28]. We then defined 15 different fitness regimes on the same underlying genotype space, each representing the selective effect of one of 15 β-lactam antibiotics (Table 1)[25]. We used this well-studied *E. coli* model system because it is one of the few microbial cell populations for which a combinatorially complete genotype-phenotype mapping has been measured[25,28]. By simulating an evolving *E. coli* cell population using the described fitness landscape paradigm, we were able to define an optimization problem on which to train RL agents (**Fig 1**).

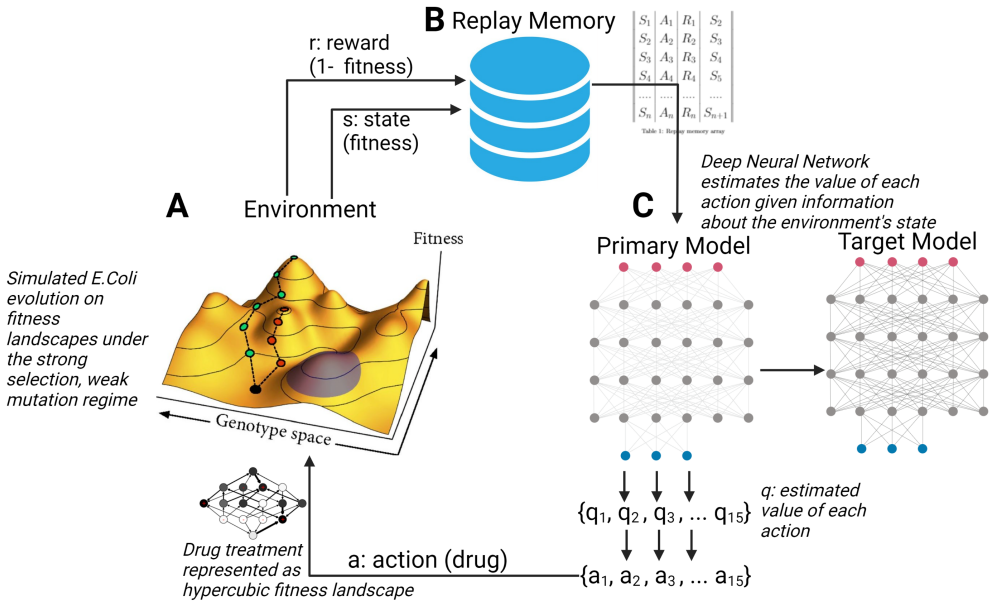

Figure 1. **Schematic of artificial intelligence system for controlling evolving cell populations. A:** *E. coli* population evolving on fitness landscapes under the strong selection, weak mutation evolutionary regime. At each time step, a reward signal r and a measure of system state s are sent to the replay memory structure. **B:** Replay memory array stores (s, a, r, s') tuples where s' is state s+1. These are then used to batch train the neural network. **C:** Deep Neural network estimates the value of each action given information about the environment's state. The action with the largest estimated value is then applied to the evolving cell population.

1.1 Simulation of Evolution Using Fitness Landscapes

We use a previously described fitness-landscape based model of evolution[15,26]. In brief, we begin by modeling an evolving asexual haploid population with N mutational sites. Each site can have one of two alleles (0 or 1). We can therefore represent the genotype of a population using an N-length binary sequence, for a total of 2^N possible genotypes. We can model theoretical drug interventions by defining fitness as a function of genotype. These "drugs" can then be represented using N-dimensional hyper-cubic graphs (**Fig 1A**). Further, if we assume that drug evolution under drug treatment follows the strong selection and weak mutation paradigm, we can then compute the probability of mutation between adjacent genotypes and represent each landscape as a Markov chain as described by Nichol et al.[15]. At each time step, we sampled from the probability distribution defined by the Markov chain to simulate the evolutionary course of a single population.

1.2 Optimization approaches

We applied two related optimization approaches to identify effective drug cycling policies in this setting. First, we extended the Markov chain framework to formulate a complete Markov Decision Process (MDP). An MDP is a discrete-time framework for modeling optimal decision-making[33]. Critically, the system under study must be partially under the control of the decision-making agent. MDPs can be solved using dynamic programming to generate optimal policies for the defined control problem[33]. The dynamic programming algorithm requires perfect information (e.g. the complete transition matrix and instantaneous state from the MDP) in order to yield optimal policies. Next, we trained agents with imperfect information using reinforcement learning to approximate a clinical scenario where perfect information will never be available. Notably, the state set, action set, and reward assignment were shared between the perfect and imperfect information conditions. The action set corresponded to the drugs available to the optimization process. We considered this system to have a finite time horizon (20 evolutionary steps in the base case). We chose a finite time horizon rather than an infinite time horizon assumption in order to more faithfully represent clinical disease courses. For our purposes, we assume that one evolutionary time step is the equivalent of one day of evolution.

1.2.1 Perfect Information

The state set S represents all potential genotypes (16 total in our base case) that the evolving population can explore. The action set A corresponds to the 15 available β-lactam antibiotics. Finally, we define the reward set (R) and the set of transition

probabilities (P) as a function of the current genotype s as well as the chosen action, a (eq 1):

$$\begin{aligned} R &= 1 - f(s|a) \text{ for } s \in S \text{ and } a \in A, \text{and,} \\ P &= f(s_{t+1}|s_t, a_t) \text{ for } s \in S \text{ and } a \in A. \end{aligned} \tag{1}$$

We solved the defined MDP using backwards induction, a dynamic programming approach designed to solve MDPs with finite time horizons[44], to generate an optimal drug cycling policy for each evolutionary episode. Backwards induction is used to estimate a value function $V(s)$ which estimates the discounted reward of being in each state s. Optimal policies $\Pi(s)$ are then inferred from the value function. Throughout the remainder of the paper we will refer to this optimal drug cycling policy as the "MDP" condition.

1.2.2 Imperfect Information

In order to assess the viability of developing optimal drug therapies from potentially clinically available information, we trained a Deep Q learner to interact with the evolving *E. Coli* system described above. Deep Q learning is an extremely well-studied and characterized method of reinforcement learning, and is particularly suited to situations where very little *a priori* knowledge about the environment is available[33,45]. We used two different training inputs to model a gradient of information loss. In the first condition, termed RL-genotype, the instantaneous genotype of the population was provided as the key training input at each time point. For this condition, the neural architecture was composed of an input layer, two 1d convolutional layers, a max pooling layer, a dense layer with 28 neurons, and an output layer with a linear activation function.

In the second condition, termed RL-fit, instantaneous population fitness of the population was provided as the key training input at each time point. The neural architecture of RL-fit was composed of a neural network with an input layer, two dense hidden layers with 64 and 28 neurons, and an output layer with a linear activation function. RL-fit takes population fitness at time t and one-hot encoded action at time $t-1$ as inputs and outputs Q-values. Q-values are estimates of the future value of a given action. Q-value estimates are improved by minimizing the temporal difference between Q-values computed by the current model and a target model, which has weights and biases that are only updated rarely. We used mean squared error (MSE) as the loss function.

We further explored the effect of information content on learned policy effectiveness by introducing a noise parameter. With noise active, fitness values $s \in S$ that were used as training inputs were first adjusted according to:

$$s_t = s_t + w \;\in\; W \sim \mathcal{N}(\mu, 0.05 \times \sigma^2). \tag{2}$$

For the noise experiment, μ was set to 0 such that $\sigma^2 = 0$ would introduce no noise. We then varied σ^2 (referred to as 'noise parameter') from 0 (no noise) to 100 (profound loss of signal fidelity).

All code and data needed to define and implement the evolutionary simulation and reinforcement learning framework can be found at https://github.com/DavisWeaver/evo_dm. The software can be installed in your local python environment using 'pip install git+https://github.com/DavisWeaver/evo_dm.git'

2 Results

In this study, we explored the viability of developing effective drug cycling policies for antibiotic treatment given less and less information about the evolving system. To this end, we developed a reinforcement learning framework to design policies that limit the growth of an evolving *E. Coli* population *in silico*. We evaluated this system in a well-studied *E. coli* system for which empirical fitness landscapes for 15 antibiotics are available in the literature[25]. A given RL agent could select from any of these 15 drugs when designing a policy to minimize population fitness. We defined three experimental conditions. In the first, we solved a Markov decision process formulation of the optimization problem under study. In doing so, we generated true optimal drug cycling policies given perfect information of the underlying system (described in **Section 1.1**). In the second, RL agents were trained using the current genotype of the simulated *E. Coli* population under selection (RL-genotype). Stepping further down the information gradient, RL agents were trained using only observed fitness of the *E. Coli* population (RL-fit). Finally, we introduced noise into these measures of observed fitness to simulate real-world conditions where only imprecise proxy measures of the true underlying state may be available. Each experimental condition was evaluated based on its ability to minimize the fitness of the population under study. We compared these conditions to two negative controls; a drug cycling policy that selects drugs completely at random (which we will refer to as "random"), and all possible two-drug cycles (i.e AMP-AM-AMP-AM-AMP). We tested 100 replicates of RL-fit and RL-genotype against each of these conditions. Each replicate was trained for 500 episodes of 20 evolutionary steps (10000 total observations of system behavior). We chose 500

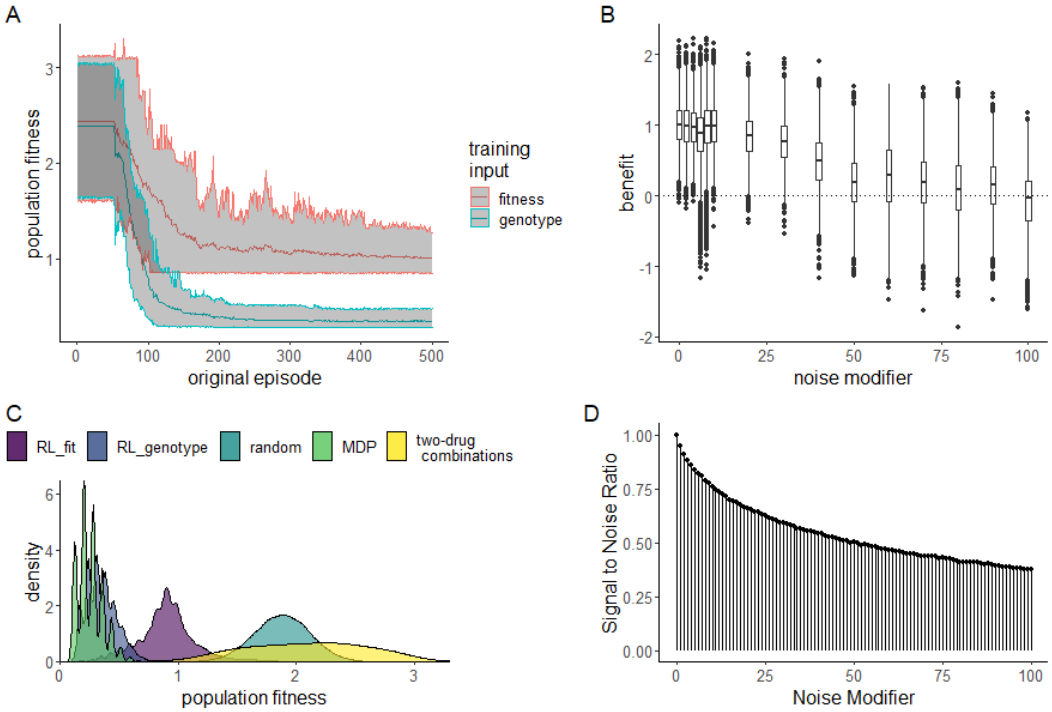

Figure 2. Performance of RL agents in a simulated *E. coli* system. **A:** Line plot showing the effectiveness of the average learned policy as training time increases on the x-axis for RL agents trained using fitness (red) or genotype (blue). **B:** Boxplot showing the effectiveness of 10 fully trained RL-fit replicates as a function of noise. Each data point corresponds to a single episode. The width of the distribution provides information about the episode by episode variability in RL-fit performance. **C:** Density plot summarizing the performance of the two experimental conditions (measured by average population fitness) relative to the three control conditions. **D:** Signal to noise ratio associated with different noise parameters. Increasing noise parameter decreases the fidelity of the signal that reaches the reinforcement learner.

episodes as the training time after extensive hyper-parameter tuning showed decreased or equal effectiveness with additional training.

Comparison of RL drug cycling policies to negative controls.

We found that both RL conditions dramatically reduced fitness relative to the random policy. In both cases, the RL conditions learned effective drug cycling policies after about 100 episodes of training and then fine-tuned them with minimal improvement through episode 500 (**Fig 2A**). As expected, RL-genotype learned a more effective drug cycling policy on average compared to RL-fit. RL-genotype had access to the instaneous state (genotype) of the evolving population, while RL-fit was only trained using a proxy measure (population fitness). In 98/100 replicates, we observed a measurable decrease in population fitness under the learned RL-fit policy versus a random drug cycling policy (**Fig S1A**). Further, we found that the average RL-fit replicate outperformed all possible two-drug cycling policies (**Fig 2C**). RL-genotype outperformed both negative controls in all 100 replicates (**Fig 2C**). In some replicates, RL-genotype achieved similar performance compared to the MDP policy (**Fig S1D**). In addition, the distribution of performance for RL-genotype policies nearly overlapped with MDP performance (**Fig 2C**). Introduction of additional noise to the training process for RL-fit led to degraded performance. However, even with a large noise modifier, RL-fit still outperformed the random drug cycling condition. With a noise modifier of 40 (fitness $+\mathcal{N}(\mu = 0, \sigma^2 = 0.05 \times 40)$), RL-fit achieved an average population fitness of 1.41 compared to 1.88 for the random drug cycling condition (**Fig 2D**).

drug sequence	replicate	condition
CTX,AMC,CTX,CPR,CTX,CPR,CTX,CPR,CTX,CPR	53	RL-fit
CTX,CPR,CPR,CPR,CTX,CPR,CPR,CPR,CTX,SAM	53	RL-genotype
CTX,AMC,CTX,AMC,CTX,AMC,CTX,AMC,CTX,CPR	23	RL-fit
CTX,AMC,CTX,AMC,CTX,AMC,CTX,AMC,CTX,AMC	23	RL-genotype
CTX,AMC,CTX,AMC,CTX,CPR,CTX,AMC,CTX,CPR	96	RL-fit
CTX,SAM,CTX,SAM,CTX,CPR,CTX,CPR,CTX,CPR	96	RL-genotype

Table 2. Example drug sequences. Here, we show the first 10 selected drugs for representative episodes of the three top-performing replicates.

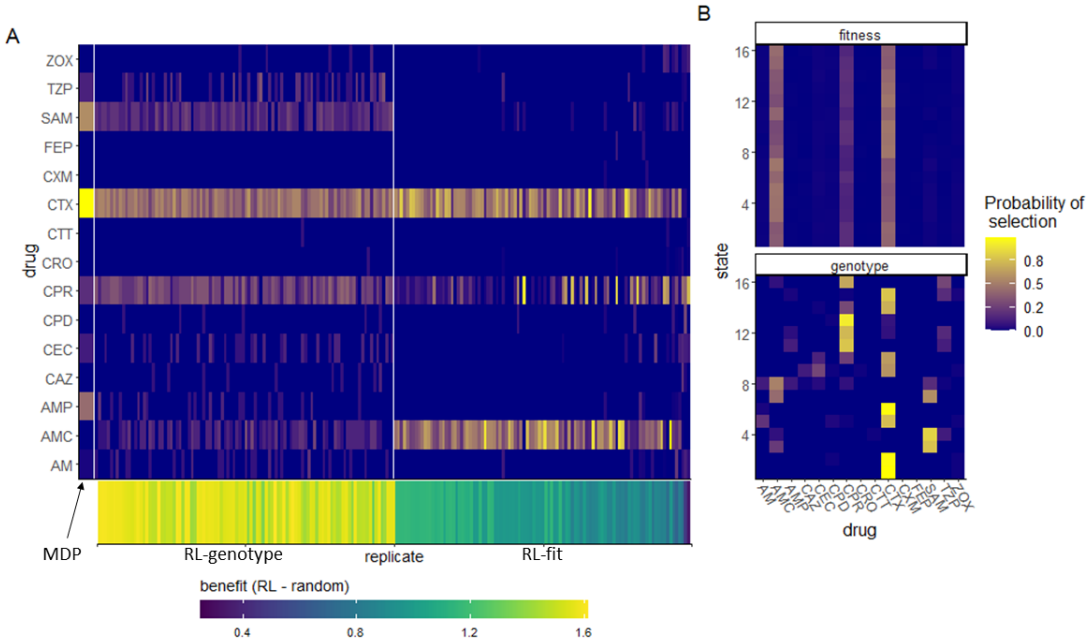

Figure 3. Drug cycling policies learned by RL-genotype and RL-fit. A: Heatmap depicting the learned policy for 100 replicates (on the x-axis) of the RL-genotype and 100 replicates of RL-fit. Far left column (enlarged) corresponds to the optimal policy derived from the MDP condition. The Y-axis describes the β-lactam antibiotics each RL agent could choose from while the color corresponds to the probability that the learned policy selected a given antibiotic. Bottom heatmap shows the median fitness benefit observed under the policy learned by a given replicate. **B:** Heatmap showing the average learned policy for RL-fit and RL-genotype. RL-genotype learns a more consistent mapping of state to action compared to RL-fit.

Overview of learned drug cycling policies for RL-fit and RL-genotype.

We evaluated the learned drug cycling policies of RL-fit, RL-genotype for the 15 β-lactam antibiotics under study. We compared these to the true optimal drug cycling policy as a reference. For this system, we show that the optimal drug cycling policy relies heavily on Cefotaxime, Ampicillin + Sulbactam, and Ampicillin (**Fig 3A**). Cefotaxime was used as treatment in more than 50% of time-steps, with Ampicillin + Sulbactam and Ampicillin used next most frequently. The optimal drug cycling policy used Cefprozil, Pipercillin + Tazobactam, and Cefaclor infrequently. The remaining drugs were not used at all. The different RL-fit replicates largely converged on a similar policy. They relied heavily on Cefotaxime and Amoxicillin + Clavulanic acid. However, they relied infrequently on Cefprozil. RL-genotype replicates also converged on a relatively conserved policy. Further, RL-genotype replicates showed a much more consistent mapping of state to action compared to RL-fit (**Fig 3B**). All optimization paradigms identified complex drug cycles that use 3 or more drugs to treat the evolving cell population. None of the tested two-drug combinations compete with policies learned by RL-genotype, and are generally out-performed by RL-fit. We show that policies that do not rely on Cefotaxime are suboptimal in this system. The three replicates that showed the least benefit compared to the random drug cycling case did not use Cefotaxime at all (**Fig 3B**). The importance of Cefotaxime is likely explained by the topography of the CTX drug landscape (**Fig S6**). More than half of the available genotypes in the CTX landscape lie in fitness valleys, providing ample opportunities to combine CTX with other drugs and "trap" the evolving population in low-fitness genotypes.

Evolutionary trajectories observed under RL-Genotype, RL-fit, and MDP drug policies.

Next, we compared the evolutionary paths taken by the simulated *E. coli* population under the MDP, RL-fit, RL-genotype, and random policy paradigms. The edge weights (corresponding to the probability of observed state transitions) of the RL-genotype and MDP landscapes show a 0.96 pearson correlation (**Fig 4**). In contrast, the edge weights of the RL-fit and MDP landscapes show a 0.82 pearson correlation (**Fig 4**). During the course of training the MDP condition, the backwards induction algorithm generated a value function $V(s,a)$ for all $s \in S$ and $a \in A$. In **Figure 4D**, we use this value function to show that certain genotypes (namely 1,5,6, and 13) were more advantageous to the evolving population than to the learner. These states were frequented much more often under the random drug cycling condition compared to any of the experimental conditions (**Fig 4D**). We also show that other genotypes (namely 12 and 11) were particularly advantageous for the learner compared to the evolving population. These states were frequented much more often under the experimental conditions compared to the random drug cycling condition (**Fig 4D**).

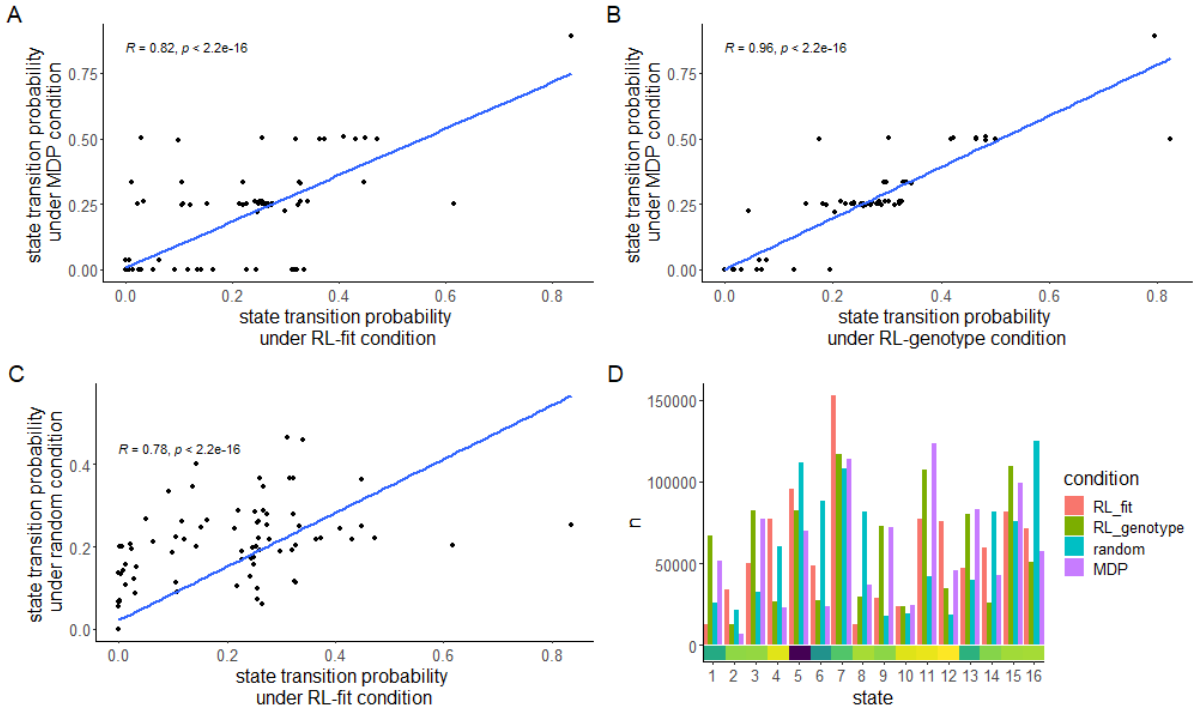

Figure 4. Comparison of evolutionary trajectories seen under different regimes A-C: Selected Pairwise comparisons of state transition frequency under different experimental conditions. State transition frequency is nearly identical for the RL-genotype and MDP conditions (R=0.97). In contrast, state-transition-frequency for the RL-fit and MDP conditions are related but less strongly correlated (R=0.75). As expected, state transition frequency is not very similar between the RL-fit and random conditions (R=0.62). **D:** Bar chart comparing the frequency that states are observed under different experimental conditions. The value of each state (to the learner) is highlighted for each state by the bottom heatmap. High value states are observed more frequently in RL-fit, RL-genotype, and MDP conditions compared to the random condition.

We also show that certain state transitions occur more frequently than others, independent of experimental conditions. For example, the population nearly always transitioned from genotype 5 to genotype 7 (**Fig 5**). This transition highlights the way these learned policies use drug landscapes to guide evolution. Genotype 5 (0100) is a fitness peak in most of the drug landscapes used in the learned policies, and is therefore a very disadvantageous state for the controlling agent. CTX, the most commonly used drug in all effective policies, has a slightly higher peak at genotype 7 (0110), which forces the population away from genotype 5 (**Fig S4**). As another example, the evolving population very rarely transitioned from state 1 to state 9 in the RL-fit condition. This state transition occurred commonly in the MDP and RL-genotype conditions (**Fig 5**). This difference is explained by the policies shown in **Figure 3B**. Under the RL-genotype policy, CTX was selected every time the population was in state 1 (the initial condition). The CTX landscape topography allows transition to 3 of the 4 single mutants, including state 9 (1000) (**Fig S6**). Under the RL-fit policy, CTX and AMC were used in about equal proportion when the population is in state 1. Unlike the CTX landscape, the AMC landscape topography does not permit evolution from state 1 to state 9 (**Fig S6**)).

Characteristics of selected drug policies

To better understand why certain drugs were used so frequently by RL-genotype, RL-fit, and the MDP policies, we developed the concept of an "opportunity landscape". An opportunity landscape is an optimistic summation of n fitness landscapes. We computed each opportunity landscape by taking the minimum fitness value for each genotype from a given set of fitness landscapes. This simplified framework gives a sense of a potential best case scenario if the drugs in a given combination are used optimally. For example, the MDP policy relied heavily on CTX, CPR, AMP, SAM, and TZP to control the simulated *E. Coli* population. The resultant opportunity landscape (**Fig 6A**) contains only a single fitness peak, with 15/16 of the genotypes in or near fitness valleys. In **Figure 6B**, we show the actual state transitions observed during evolution under the MDP policy. We also color the nodes based on the value function estimated by solving the MDP. As expected, the value function estimated by the MDP aligns closely with the topography of the opportunity landscape. There is only one genotype that the value function scores as being very poor for the learner, corresponding to the single peak in the opportunity fitness landscape (**Fig 6**). Interestingly, the opportunity landscape predicted that the population would evolve to the single fitness peak and fix. In contrast, the observed state transitions suggest that the MDP policy was able to guide the population away from that single fitness peak. A more detailed discussion of opportunity landscapes can be found in the supplemental materials.

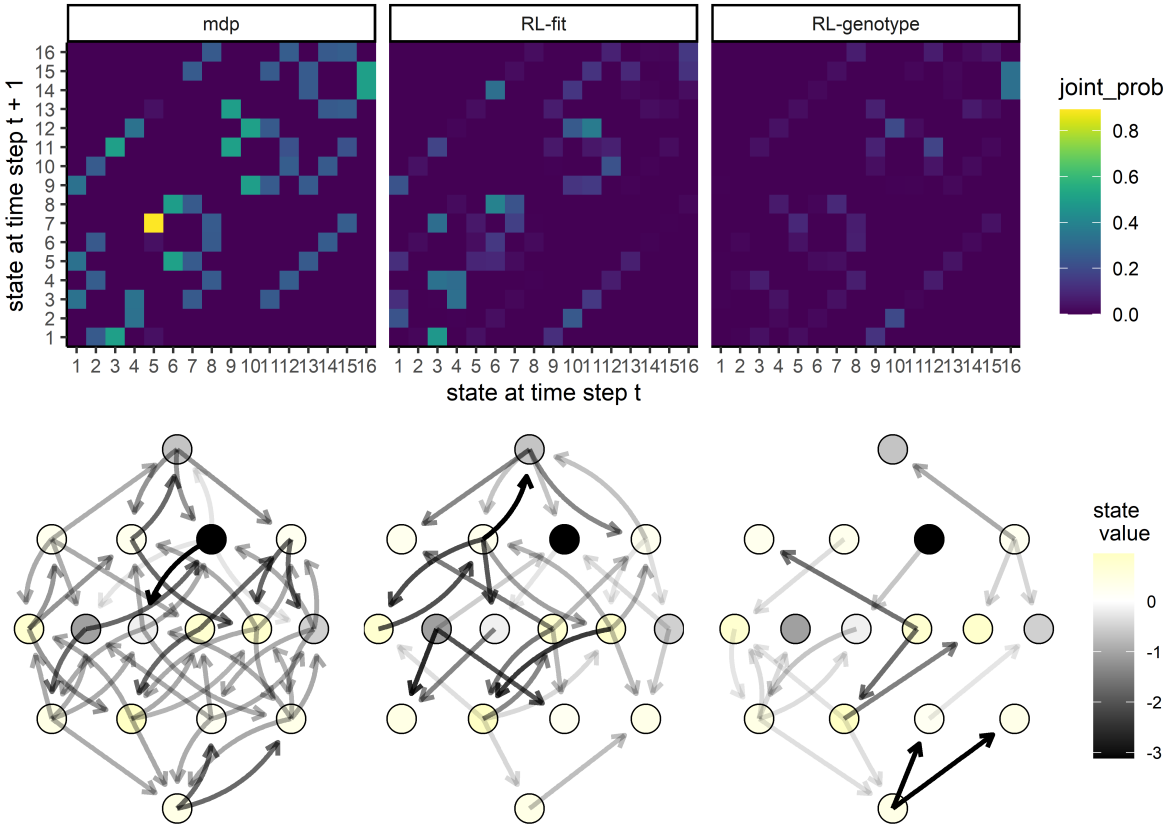

Figure 5. Movement of simulated *E. Coli* population through the genomic landscape. Top row: Heatmap depicting the joint probability distribution for each state transition under the different experimental conditions. The second two show the difference in state transition probability compared to the MDP condition. **Bottom row:** Graph depicting the fitness landscape, beginning with the wild type (bottom) all the way to the quadruple mutant (top). Size of arrow depicts the frequency with which a state transition was observed under the labeled experimental condition. The color of each node corresponds with the expected value (to the learner) of being in that state. As above, the second two arrows correspond to the observed difference between RL-Fit or RL-genotype and the MDP condition.

We also show that both the MDP and RL-genotype conditions select the drug with the lowest fitness for most genotypes (**Fig 6C**). There are a few notable exceptions to this rule, which highlight RL-genotype's capacity for treatment planning. A greedy policy that selects the lowest drug-fitness combination for every genotype would select Amoxicillin (AM) when the population is identified as being in genotype 5. The AM drug landscape then strongly favors transition back to the wild-type genotype (state 1). From state 1, most available drugs encourage evolution back to the genotype 5 fitness peak. As we see in **Figure 6B**, state 5 is by far the least advantageous for the learner. The greedy policy therefore creates an extremely disadvantageous cycle of evolution. In fact, none of the tested policies rely heavily on AM in state 5 (**Fig 3B**), instead taking a fitness penalty to select Cefotaxime (CTX). The CTX drug landscape encourages evolution to the double mutant, which has access to the highest value areas of the landscape. Finally, we rank drug landscapes based on the number of genotypes with a fitness value < 1 (**Fig 6D**). Based on the defined reward function, these genotypes would be considered advantageous to the learner. We show that drugs identified as useful by the optimal policy or RL-genotype tend to have more advantageous genotypes in their drug landscape. The only two highly permissive landscapes (CPD, CPR) that aren't used have extremely similar topography to CTX, which most policies were built around.

3 Discussion

The evolution of widespread microbial drug resistance is driving a growing public health crisis around the world. In this study, we show a proof of concept for how existing drugs could be leveraged to control microbial populations without increasing drug resistance. To that end, we tested optimization approaches given decreasing amounts of information about an evolving system of *E.Coli*, and showed that it is possible to learn highly effective drug cycling policies given only empirically measurable information. To accomplish this, we developed a novel reinforcement learning approach to control an evolving population of *E. Coli in silico*. We focused on 15 empirically measured fitness landscapes pertaining to different clinically available β-lactam

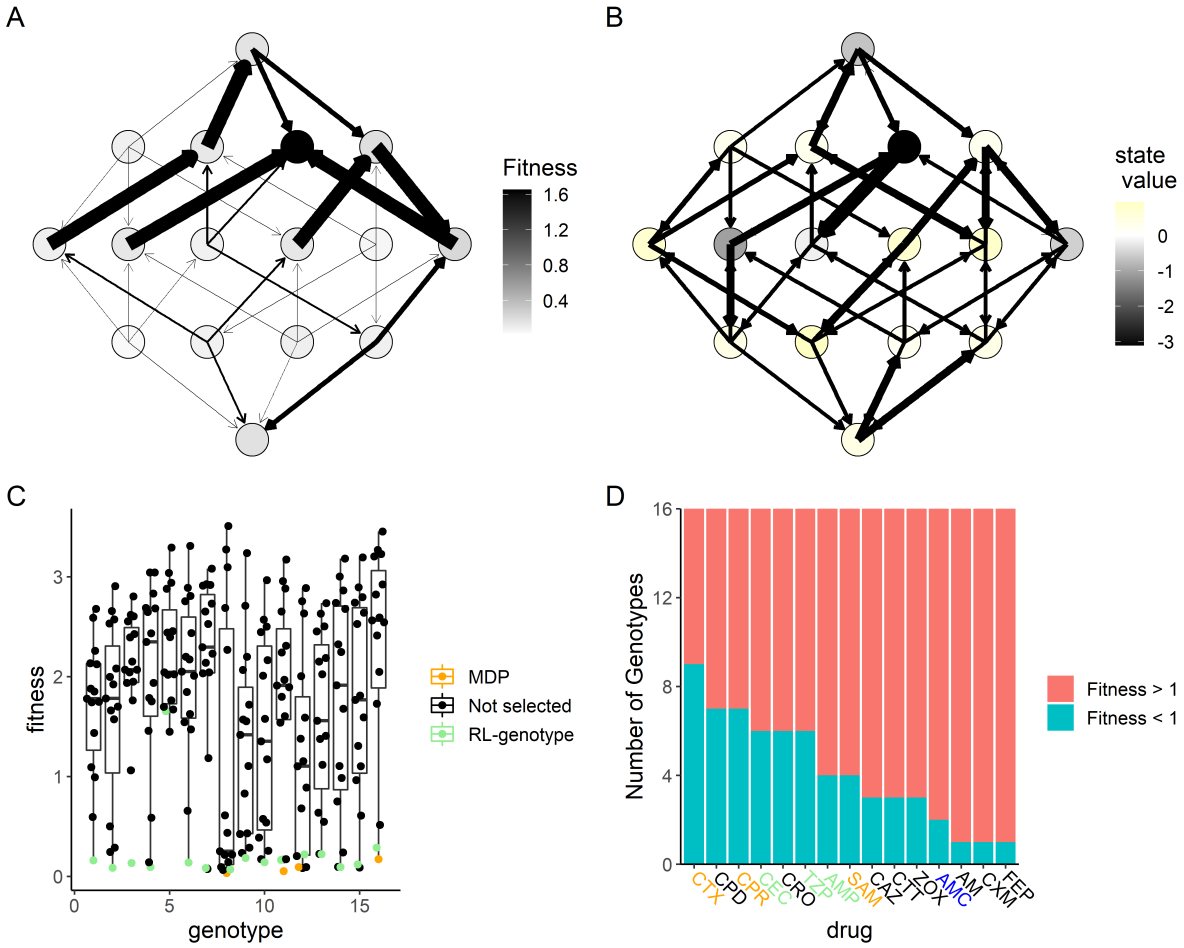

Figure 6. MDP value function closely matches opportunity landscape for drugs commonly used under MDP policy. Panels A and B show the 16-genotype fitness landscape under study, starting with the wild type at the top, progressing throw the single mutants, double mutants, triple mutants, and finally the quadruple mutant at the bottom. **A:** Opportunity landscape for the 5 drugs most commonly used under the MDP policy (CTX, CPR, AMP, SAM, and TZP). **B:** Observed state transitions under the MDP policy. The node color corresponds to the value function estimated by solving the MDP. Lower values correspond to states the MDP policy attempts to avoid while higher values correspond to states the MDP policy attempts to steer the population. **C:** Scatter Plot showing the distribution of fitness with respect to genotype for the 15 β -lactam antibiotics under study. The drug selected by RL-genotype in a given genotype is highlighted in light blue. In cases where the MDP selected a different drug than RL-genotype, that drug is highlighted in orange. **D:** Number of genotypes with fitness above or below 1 for each drug under study. Drugs that are used by both the MDP and RL-genotype are highlighted in orange. Drugs that are used by only the MDP are highlighted in green. Drugs that are used by only RL-genotype are highlighted in blue.

antibiotics (**Table 1**). In this setting, RL agents selected treatments that, on average, controlled population fitness much more effectively than either of the two negative controls. We showed that RL agents with access to the instantaneous genotype of the population over time approach the MDP-derived optimal policy for these landscapes. Critically, we showed that RL agents were capable of developing effective drug cycling protocols even when the measures of fitness used for training were first adjusted by a noise parameter. This suggests that even imperfect measurements of an imperfect measure of population state (the kind of measurements we are able to make in clinical settings) may be sufficient to develop effective control policies. We also show that RL or MDP-derived policies consistently outperform simple alternating drug cycling policies. Finally, we introduced the concept of the "Opportunity Landscape" which can provide powerful intuition into the viability of various drug combinations.

Our work expands a rich literature on the subject of evolutionary control through formal optimization approaches. Our group and others have developed and optimized perfect information systems to generate effective drug cycling policies[11,12,14,16,17]. Further, a limited number of studies have used RL-based methods for the development of clinical optimization protocols[20,38–41,43]. These studies have been limited so far to contrived simulated systems, including a recent study that introduced Celludose, a RL framework capable of controlling evolving bacterial populations in a stochastic simulated system[42].

Much like the studies noted above, we show that AI or MDP-based policies for drug selection or drug dosing dramatically outperform sensible controls in the treatment of an evolving cell population. We also extend this literature in two key ways. To our knowledge, ours is the first optimization protocol capable of learning effective drug cycling policies using only observed population fitness (a clinically tractable measure) as the key training input. Second, we grounded our work with empirically measured fitness landscapes which will facilitate more natural extension to the bench.

There are several limitations to this work which bear mention. We assume that selection under drug therapy represents a strong-selection and weak mutation regime in order to compute transition matrices for our models. While this is likely true in most cases, it is possible that other selection regimes emerge in cases of real world pharmacokinetics where the drug concentration fluctuates dramatically. In addition, we chose to keep drug concentration constant throughout are analysis, largely owing to the lack of robust empirical data linking genotype to phenotype under dose varying conditions (sometimes called a fitness seascape)[46]. As more empirical fitness seascape data becomes available, a natural extension would be to explore the efficacy of the RL system in controlling a population by varying both drug and dose.

While we present the most extensive genotype-phenotype modeling work to date on this subject, we still only modeled the effect of mutations at 4 genotypic positions. The real *E. Coli* genome is approximately 5×10^6 base pairs[47]. The evolutionary landscape for living organisms is staggeringly large, and not tractable to model *in silico*. It is possible that empirical measures of fitness like growth rate or cell count may not provide a robust enough signal of the underlying evolutionary state on real genomes. *In vitro* implementations of reinforcement learning-based drug cycle optimization systems are needed to address this potential shortcoming. Another potential alternative would be to use the comparatively low-dimensional phenotype landscape of drug resistance[48].

In this work, we present a novel reinforcement-learning framework capable of controlling an evolving population of *E. Coli in silico*. We show that RL agents stably learn multi-drug combinations that were state specific and reliably out-performed a random drug cycling policy as well as all possible two-drug cycling policies. We also highlight key features of the types of drug landscapes that are useful for the design of evolutionary control policies. Our work represents an important proof-of-concept for AI-based evolutionary control, an emerging field with the potential to revolutionize clinical medicine.

Acknowledgements

This work was made possible by the National Institute of Health (5R37CA244613-03, 5T32GM007250-46, and T32CA094186) and American Cancer Society (RSG-20-096-01). Figure 1 was created with BioRender.com.

References

1. Murray, C. J. *et al.* Global burden of bacterial antimicrobial resistance in 2019: a systematic analysis. *The Lancet* **399**, 629–655, DOI: 10.1016/S0140-6736(21)02724-0 (2022). Publisher: Elsevier.
2. Centers for Disease Control and Prevention (U.S.). Antibiotic resistance threats in the United States, 2019. Tech. Rep., Centers for Disease Control and Prevention (U.S.) (2019). DOI: 10.15620/cdc:82532.
3. Plackett, B. Why big pharma has abandoned antibiotics. *Nature* **586**, DOI: 10.1038/d41586-020-02884-3 (2020).
4. Stearns, S. C. Evolutionary medicine: Its scope, interest and potential. *Proc. Royal Soc. B: Biol. Sci.* **279**, 4305–4321, DOI: 10.1098/rspb.2012.1326 (2012).
5. Grunspan, D. Z., Nesse, R. M., Barnes, M. E. & Brownell, S. E. Core principles of evolutionary medicine. *Evol. Medicine, Public Heal.* **2018**, 13–23, DOI: 10.1093/emph/eox025 (2018).
6. Perry, G. H. Evolutionary medicine. *eLife* **10**, e69398, DOI: 10.7554/eLife.69398 (2021).
7. Andersson, D. I. *et al.* Antibiotic resistance: turning evolutionary principles into clinical reality. *FEMS Microbiol. Rev.* **44**, 171–188 (2020). Publisher: Oxford University Press.
8. Manrubia, S. *et al.* From genotypes to organisms: State-of-the-art and perspectives of a cornerstone in evolutionary dynamics. *Phys. Life Rev.* **38**, 55–106, DOI: 10.1016/j.plrev.2021.03.004 (2021).
9. Stracy, M. *et al.* Minimizing treatment-induced emergence of antibiotic resistance in bacterial infections. *Science* **375**, 889–894, DOI: 10.1126/science.abg9868 (2022). Publisher: American Association for the Advancement of Science.
10. Baym, M., Stone, L. K. & Kishony, R. Multidrug evolutionary strategies to reverse antibiotic resistance. *Science* **351**, aad3292 (2016). Publisher: American Association for the Advancement of Science.
11. Yoon, N., Vander Velde, R., Marusyk, A. & Scott, J. G. Optimal Therapy Scheduling Based on a Pair of Collaterally Sensitive Drugs. *Bull. Math. Biol.* **80**, 1776–1809, DOI: 10.1007/s11538-018-0434-2 (2018).
12. Maltas, J. & Wood, K. B. Pervasive and diverse collateral sensitivity profiles inform optimal strategies to limit antibiotic resistance. *PLoS biology* **17**, e3000515, DOI: 10.1371/journal.pbio.3000515 (2019).
13. Maltas, J. & Wood, K. B. Dynamic collateral sensitivity profiles highlight challenges and opportunities for optimizing antibiotic sequences. *bioRxiv* (2021).
14. Gluzman, M., Scott, J. G. & Vladimirsky, A. Optimizing adaptive cancer therapy: dynamic programming and evolutionary game theory. *Proc. Royal Soc. B: Biol. Sci.* **287**, 20192454, DOI: 10.1098/rspb.2019.2454 (2020). Publisher: Royal Society.
15. Nichol, D. *et al.* Steering Evolution with Sequential Therapy to Prevent the Emergence of Bacterial Antibiotic Resistance. *PLOS Comput. Biol.* **11**, e1004493, DOI: 10.1371/journal.pcbi.1004493 (2015). Publisher: Public Library of Science.
16. Yoon, N., Krishnan, N. & Scott, J. Theoretical modeling of collaterally sensitive drug cycles: shaping heterogeneity to allow adaptive therapy. *J. Math. Biol.* **83**, 47, DOI: 10.1007/s00285-021-01671-6 (2021).
17. Iram, S. *et al.* Controlling the speed and trajectory of evolution with counterdiabatic driving. *Nat. Phys.* **17**, 135–142, DOI: 10.1038/s41567-020-0989-3 (2021). Bandiera_abtest: a Cg_type: Nature Research Journals Number: 1 Primary_atype: Research Publisher: Nature Publishing Group Subject_term: Biophysics;Statistical physics;Theoretical physics Subject_term_id: biophysics;statistical-physics;theoretical-physics.
18. Maltas, J., Singleton, K. R., Wood, K. C. & Wood, K. B. Drug dependence in cancer is exploitable by optimally constructed treatment holidays. *bioRxiv* (2022).
19. Chakrabarti, S. & Michor, F. Pharmacokinetics and drug interactions determine optimum combination strategies in computational models of cancer evolution. *Cancer Res.* **77**, 3908–3921, DOI: 10.1158/0008-5472.CAN-16-2871 (2017).
20. Newton, P. K. & Ma, Y. Nonlinear adaptive control of competitive release and chemotherapeutic resistance. *Phys. Rev. E* **99**, 022404, DOI: 10.1103/PhysRevE.99.022404 (2019).
21. Kim, S., Lieberman, T. D. & Kishony, R. Alternating antibiotic treatments constrain evolutionary paths to multidrug resistance. *Proc. Natl. Acad. Sci.* **111**, 14494–14499, DOI: 10.1073/pnas.1409800111 (2014). Publisher: Proceedings of the National Academy of Sciences.
22. Zhang, J., Cunningham, J. J., Brown, J. S. & Gatenby, R. A. Integrating evolutionary dynamics into treatment of metastatic castrate-resistant prostate cancer. *Nat. Commun.* **8**, DOI: 10.1038/s41467-017-01968-5 (2017).

23. Cunningham, J. J., Brown, J. S., Gatenby, R. A. & Staňková, K. Optimal control to develop therapeutic strategies for metastatic castrate resistant prostate cancer. *J. Theor. Biol.* **459**, 67–78, DOI: 10.1016/j.jtbi.2018.09.022 (2018).

24. Weinreich, D. M., Watson, R. A. & Chao, L. Perspective: Sign Epistasis and Genetic Costraint on Evolutionary Trajectories. *Evolution* **59**, 1165–1174, DOI: 10.1111/j.0014-3820.2005.tb01768.x (2005). _eprint: https://onlinelibrary.wiley.com/doi/pdf/10.1111/j.0014-3820.2005.tb01768.x.

25. Mira, P. M. *et al.* Rational Design of Antibiotic Treatment Plans: A Treatment Strategy for Managing Evolution and Reversing Resistance. *PLOS ONE* **10**, e0122283, DOI: 10.1371/journal.pone.0122283 (2015). Publisher: Public Library of Science.

26. Maltas, J., McNally, D. M. & Wood, K. B. Evolution in alternating environments with tunable inter-landscape correlations. *Evol. international journal organic evolution* **75**, 10–24, DOI: 10.1111/evo.14121 (2021).

27. de Visser, J. A. G. M. & Krug, J. Empirical fitness landscapes and the predictability of evolution. *Nat. Rev. Genet.* **15**, 480–490, DOI: 10.1038/nrg3744 (2014). Bandiera_abtest: a Cg_type: Nature Research Journals Number: 7 Primary_atype: Reviews Publisher: Nature Publishing Group Subject_term: Epistasis;Evolutionary genetics;Experimental evolution Subject_term_id: epistasis;evolutionary-genetics;experimental-evolution.

28. Weinreich, D. M., Delaney, N. F., Depristo, M. A. & Hartl, D. L. Darwinian evolution can follow only very few mutational paths to fitter proteins. *Sci. (New York, N.Y.)* **312**, 111–114, DOI: 10.1126/science.1123539 (2006).

29. Ogbunugafor, C. B., Wylie, C. S., Diakite, I., Weinreich, D. M. & Hartl, D. L. Adaptive Landscape by Environment Interactions Dictate Evolutionary Dynamics in Models of Drug Resistance. *PLoS Comput. Biol.* **12**, 1–20, DOI: 10.1371/journal.pcbi.1004710 (2016).

30. Toprak, E. *et al.* Evolutionary paths to antibiotic resistance under dynamically sustained drug selection. *Nat. genetics* **44**, 101–105 (2012). Publisher: Nature Publishing Group.

31. Greenbury, S. F., Louis, A. A. & Ahnert, S. E. The structure of genotype-phenotype maps makes fitness landscapes navigable. *Nat. Ecol. & Evol.* 1–11, DOI: 10.1038/s41559-022-01867-z (2022). Publisher: Nature Publishing Group.

32. Baym, M. *et al.* Spatiotemporal microbial evolution on antibiotic landscapes. *Sci. (New York, N.Y.)* **353**, 1147–1151, DOI: 10.1126/science.aag0822 (2016).

33. Sutton, R. S. & Barto, A. G. *Reinforcement learning: An introduction* (MIT press, 2018).

34. Du Plessis, L., Leventhal, G. E. & Bonhoeffer, S. How good are statistical models at approximating complex fitness landscapes? *Mol. biology evolution* **33**, 2454–2468 (2016). Publisher: Oxford University Press.

35. Silver, D. *et al.* Mastering the game of Go with deep neural networks and tree search. *Nature* **529**, DOI: 10.1038/nature16961 (2016).

36. Mnih, V. *et al.* Human-level control through deep reinforcement learning. *Nature* **518**, 529–533, DOI: 10.1038/nature14236 (2015). Bandiera_abtest: a Cg_type: Nature Research Journals Number: 7540 Primary_atype: Research Publisher: Nature Publishing Group Subject_term: Computer science Subject_term_id: computer-science.

37. Vinyals, O. *et al.* Grandmaster level in StarCraft II using multi-agent reinforcement learning. *Nature* **575**, 350–354, DOI: 10.1038/s41586-019-1724-z (2019). Bandiera_abtest: a Cg_type: Nature Research Journals Number: 7782 Primary_atype: Research Publisher: Nature Publishing Group Subject_term: Computer science;Statistics Subject_term_id: computer-science;statistics.

38. Moore, B. L. *et al.* Reinforcement Learning for Closed-Loop Propofol Anesthesia: A Study in Human Volunteers. *J. Mach. Learn. Res.* **15**, 655–696 (2014).

39. Petersen, B. K. *et al.* Deep Reinforcement Learning and Simulation as a Path Toward Precision Medicine. *J. Comput. Biol. A J. Comput. Mol. Cell Biol.* **26**, 597–604, DOI: 10.1089/cmb.2018.0168 (2019).

40. Padmanabhan, R., Meskin, N. & Haddad, W. M. Reinforcement learning-based control of drug dosing for cancer chemotherapy treatment. *Math. Biosci.* **293**, 11–20, DOI: 10.1016/j.mbs.2017.08.004 (2017).

41. Ahn, I. & Park, J. Drug scheduling of cancer chemotherapy based on natural actor-critic approach. *Bio Syst.* **106**, 121–129, DOI: 10.1016/j.biosystems.2011.07.005 (2011).

42. Engelhardt, D. Dynamic Control of Stochastic Evolution: A Deep Reinforcement Learning Approach to Adaptively Targeting Emergent Drug Resistance. *J. Mach. Learn. Res.* **21**, 1–30 (2020).

43. Martin, R. B. Optimal control drug scheduling of cancer chemotherapy. *Automatica* **28**, 1113–1123, DOI: 10.1016/0005-1098(92)90054-J (1992).

44. Kallenberg, L. *Lecture Notes Markov Decision Problems - version 2020* (2020).

45. Arulkumaran, K., Deisenroth, M. P., Brundage, M. & Bharath, A. A. Deep reinforcement learning: A brief survey. *IEEE Signal Process. Mag.* **34**, 26–38, DOI: 10.1109/MSP.2017.2743240 (2017).

46. King, E. S. *et al.* Fitness seascapes facilitate the prediction of therapy resistance under time-varying selection, DOI: 10.1101/2022.06.10.495696 (2022). Pages: 2022.06.10.495696 Section: New Results.

47. Rode, C. K., Melkerson-Watson, L. J., Johnson, A. T. & Bloch, C. A. Type-Specific Contributions to Chromosome Size Differences in Escherichia coli. *Infect. Immun.* **67**, 230–236 (1999).

48. Iwasawa, J. *et al.* Analysis of the evolution of resistance to multiple antibiotics enables prediction of the Escherichia coli phenotype-based fitness landscape. *PLOS Biol.* **20**, e3001920, DOI: 10.1371/journal.pbio.3001920 (2022). Publisher: Public Library of Science.

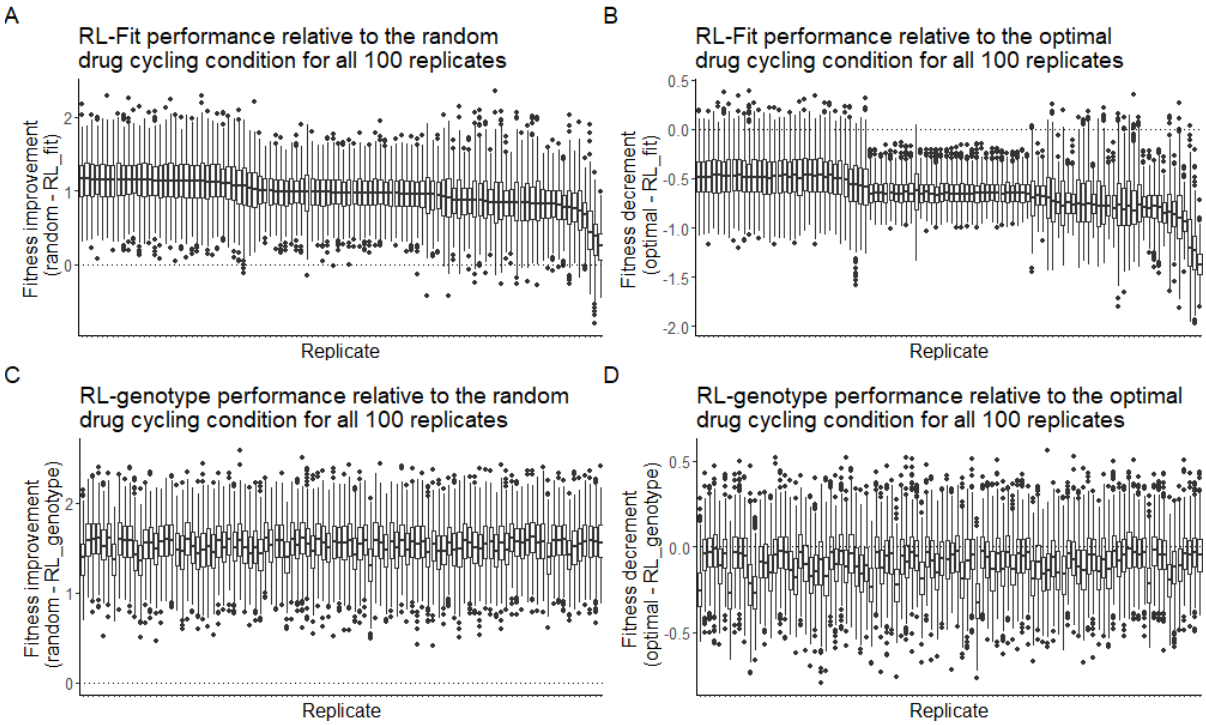

Figure S1. Performance of RL-fit and RL-genotype for each replicate. A: Fitness observed under RL-fit policy compared to random drug cycling condition. **B:** Fitness observed under RL-fit policy compared to fitness observed under optimal policy. **C:** Fitness observed under RL-genotype policy compared to random drug cycling condition. **D:** Fitness observed under RL-genotype policy compared to fitness observed under optimal policy.

Supplemental Materials

1.1 Hyperparameter tuning

We varied key hyperparameters one at a time in order to identify optimal values to promote learning in this setting. Parameter ranges and the selected value are shown in **Table S1**. Due to the long run-times of the training process, we were unable to make use of more formal hyper-parameter optimization approaches. Future work will increase the efficiency of training reinforcement learners in this setting, opening up a number of interesting follow-on studies.

1.2 Additional performance data for RL agents

As mentioned in the main text, we tested both the RL-fit and RL-genotype conditions 100 times each. In **Figure S1**, we show the perfomance of all 100 RL-fit and RL-genotype replicates. In 98/100 replicates, RL-fit outperformed the random drug cycling case (**Fig S1A**). The very best RL-fit replicates still fell short of the MDP-derived optimal policy (**Fig S1B**). In all 100 replicates, RL-genotype outperformed the random drug cycling case ((**Fig S1C**). RL-genotype performance approached the performance of the optimal policy (**Fig S1D**).

Table S1. Key Hyperparameters for reinforcement learner

Parameter	Value	Range
gamma	0.99	0-1
learning rate	0.0001	0.000001-0.1
minibatch size	60	20-500
update target model frequency	310	100-1000

1.3 Policy Clustering

We performed PCA on the policies for all 100 replicates from the RL-genotype and RL-fit conditions. We then used the silhouette method, implemented in the factoextra package, to estimate the appropriate number of clusters. We found that either 2 or 5 clusters would be optimal. As two clusters would only recapitulate our orignal RL-genotype and RL-fit conditions, we performed kmeans clustering with 5 centers. Results are shown in **Fig S2**.

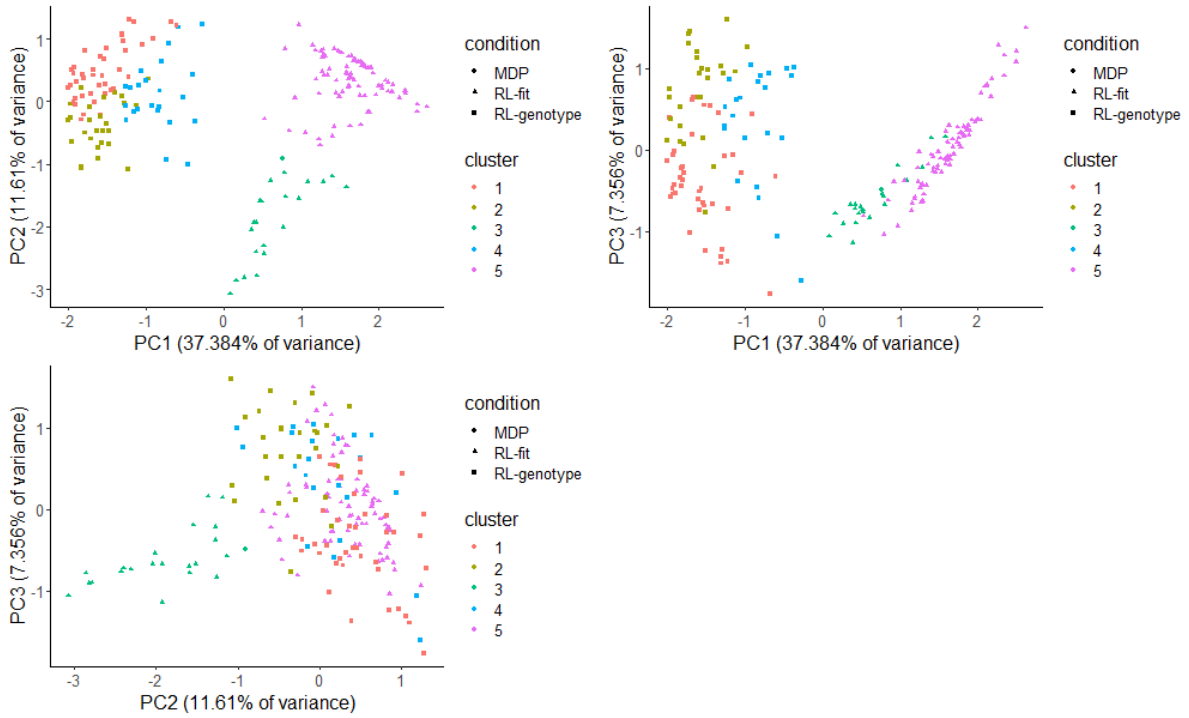

Figure S2. Identification of policy groups using PCA and kmeans clustering. RL-fit replicates were separated into 2 distinct replicates. RL-genotype replicates were separated into 3 distinct groups but it is unclear if these groups are meaningfully different.

We plotted the top 3 pairwise comparisons of principal components, which together account for about 56.4% of the variance in this dataset. The RL-fit and RL-genotype policies were clearly separated by this method, with RL-genotype being split between clusters 1,2, and 4. RL-fit was split between clusters 3 and 5 (Fig S2). Clusters 3 and 5 represent meaningfully different policy motifs that RL-fit found frequently over the course of 100 replicates. Cluster 3 replicates were Cefprozil dominant, and used Cefotaxime and Amoxicillin + Clavulanic acid infrequently. Cluster 5 replicates were Cefotaxime and Amoxicillin + Clavulanic acid dominant, and used Cefprozil infrequently (**Fig S3**). Notably, cluster 3 replicates tended to have worse performance compared to cluster 5 replicates (**Fig 3**).

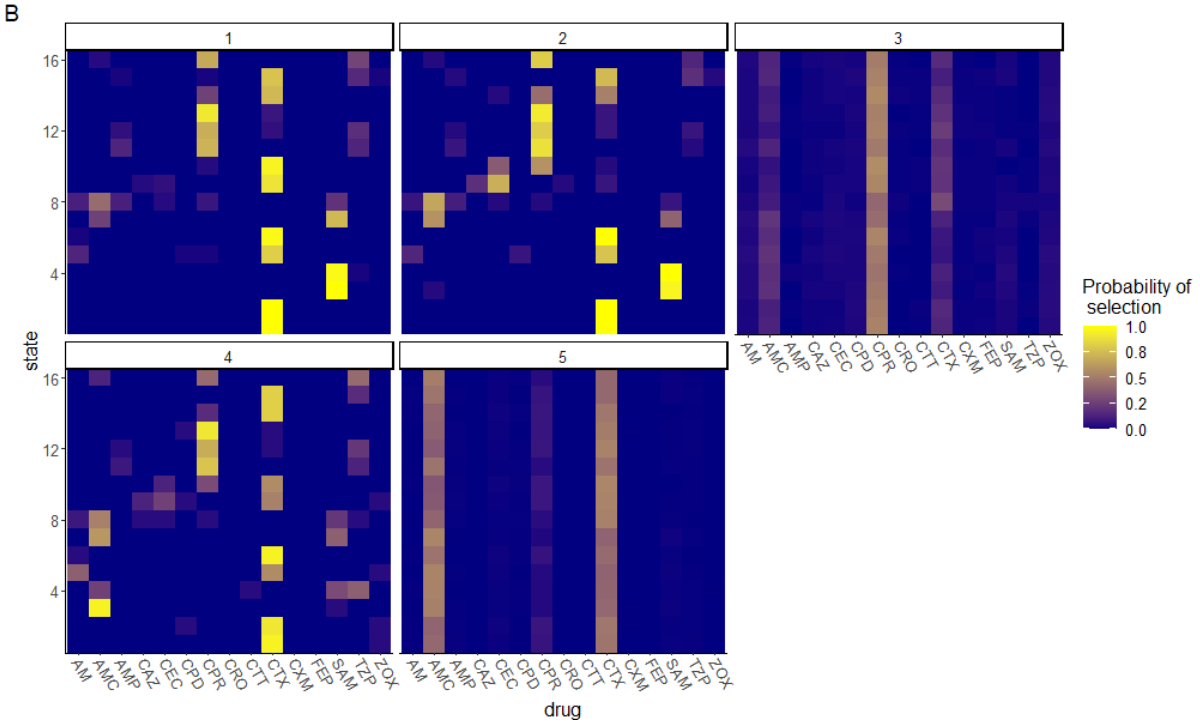

Figure S3. policy heatmaps for groups identified using PCA and kmeans clustering. Groups 1,2, and 4 correspond to RL-genotype policies. Groups 3 and 5 correspond to RL-fit policies. color gradient represents probability that a given drug (x-axis) will be selected when population is in a given state (y-axis).

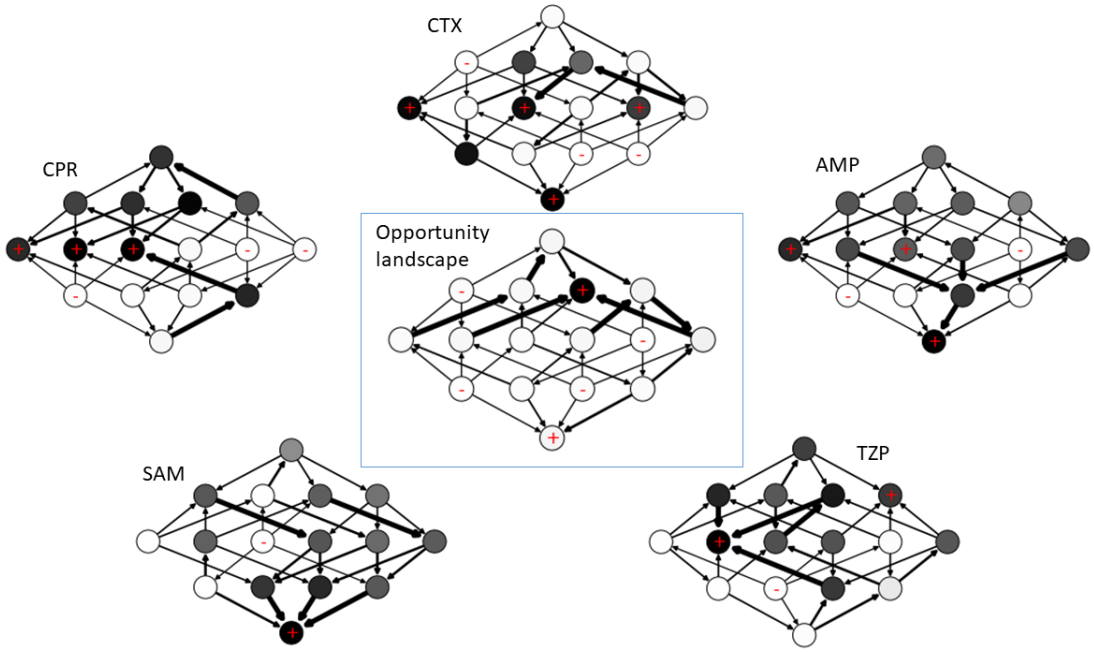

Figure S4. **Opportunity Landscape for MDP-derived policy.** Opportunity landscape is an optimistic combination of 5 empirically measured drug landscapes. Just 1/16 genotypes is near a fitness peak on the opportunity landscape, helping to explain the extremely low fitness observed in the simulated E.Coli population when the MDP-derived policy is applied.

1.4 Opportunity Landscapes

We define an opportunity landscape to be the most optimistic combination of n landscapes, formed by taking the minimum possible fitness at each genotypic position. This construct can help us better understand how the learner uses different combinations of drugs to maintain the evolving population at extremely low fitness values. Figure S4 describes the opportunity landscape discovered by the MDP condition. As noted in the main text, the MDP primarily uses 5 drugs (CTX, CPR, AMP, SAM, and TZP) in combination to trap the evolving population of E. Coli at extremely low fitness genotypes. In the combined opportunity landscape, just one genotype (0100) had a high fitness in all 5 drugs. As expected, the opportunity landscape closely matches the value function estimated by the MDP (**Fig 5**)

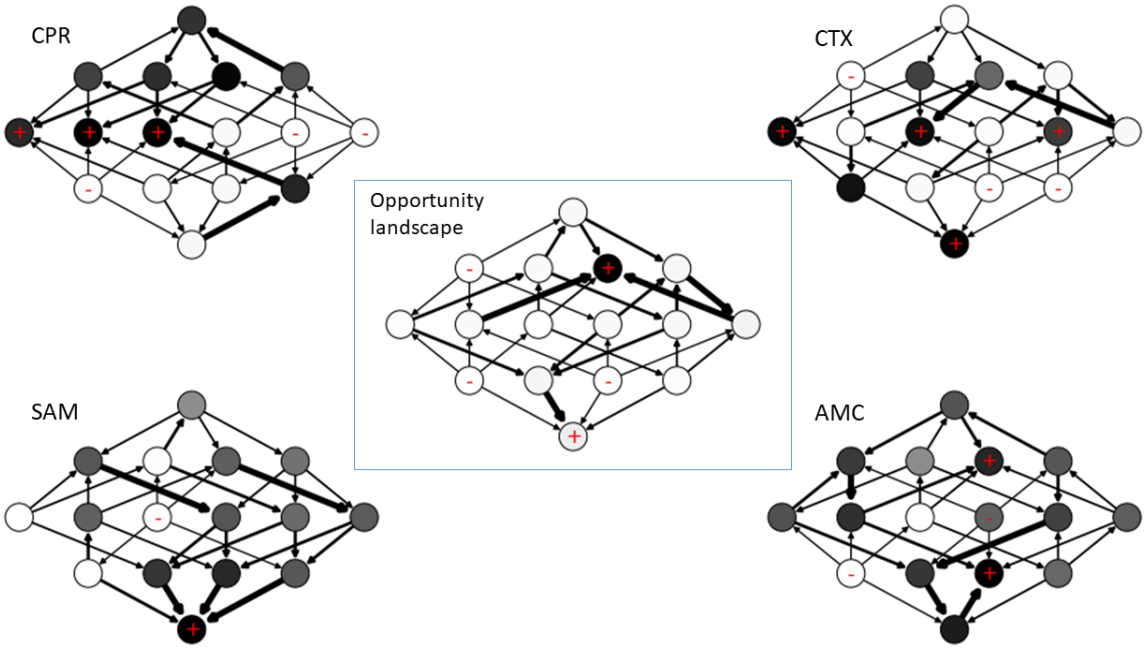

Figure S5. Opportunity landscape for most common policy identified in the RL-genotype condition. As in the MDP-derived policy, just 1/16 genotypes is near a fitness peak in the opportunity landscape.

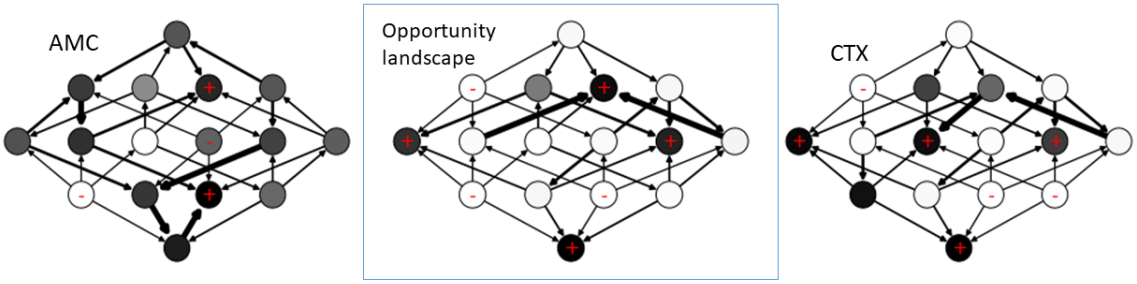

Figure S6. Opportunity landscape for the most common policy identified in the RL-fit condition. The most common RL-fit policy relies on AMC and CTX to control the E. Coli population. Assuming the most optimistic combination of these two drug landscapes, 4/16 genotypes are near a fitness peak.

The opportunity landscape for the RL-genotype is almost identical to the opportunity landscape observed for the MDP policy (**Fig S5**). Interestingly, RL-genotype only uses 3 of the 5 drugs in the MDP policy; CPR, CTX, and SAM. RL-fit discovered policies that typically only used two drugs. The most effective RL-fit policies relied heavily on AMC and CTX. We present the resulting opportunity landscape in **Figure S6**. As expected, there are more genotypes with high fitness values under this two-drug paradigm compared to the 4 or 5 drug policies discovered by RL-genotype and the MDP, respectively.

1.5 MDP policy

As mentioned in the main text, we computed the MDP policy by formulating a markov decision process of the strong selection, weak mutation model of evolution under study. We then solved the MDP using backward induction, an algorithm designed to identify an optimal policy for a finite time discrete MDP. The identified policy is a function of current state and current time step, making it even more specific than the policies identified by the reinforcement learning conditions. We show the time and state-specific MDP policy in **Figure S7**. Near the end of an episode (steps 19 and 20), we see a switch to a greedy policy that simply selects the drug with the minimum fitness for a given genotype. We also varied the discount rate (gamma), between 0 and 1 during the hyperparameter tuning process. In **Figure S8**, we show the effect of gamma on the avergage fitness achieved by the MDP policy. While gamma didn't have a large effect, likely due to the relatively short length (20 time steps) of each episode, we show that increasing gamma led to increased performance of the computed MDP policy. We also show that increasing gamma led to increased use of CTX (drug 4).

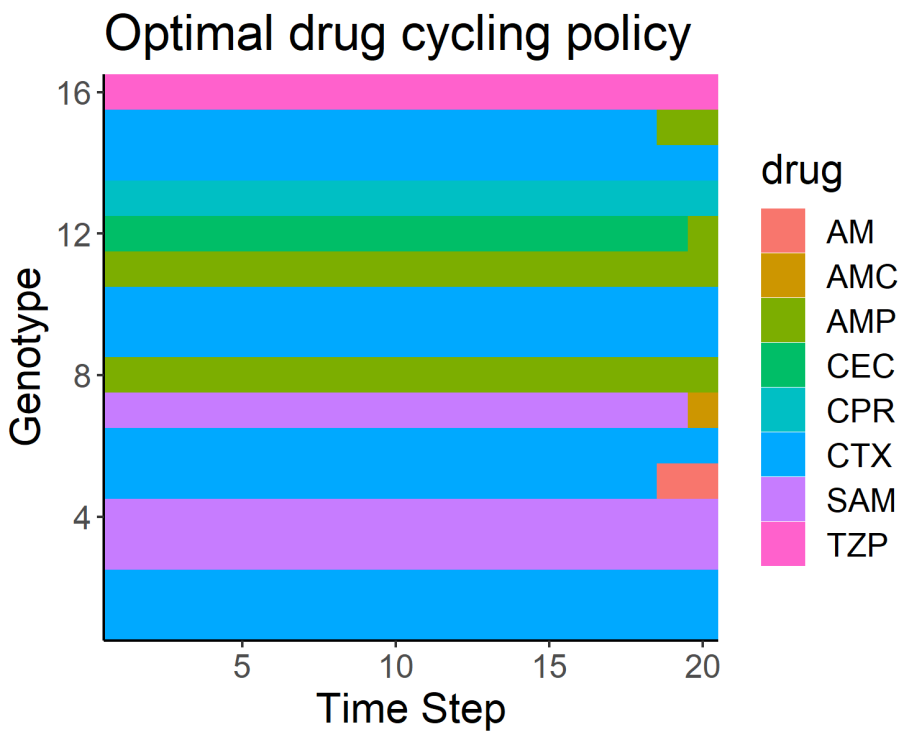

Figure S7. MDP-derived optimal policy.

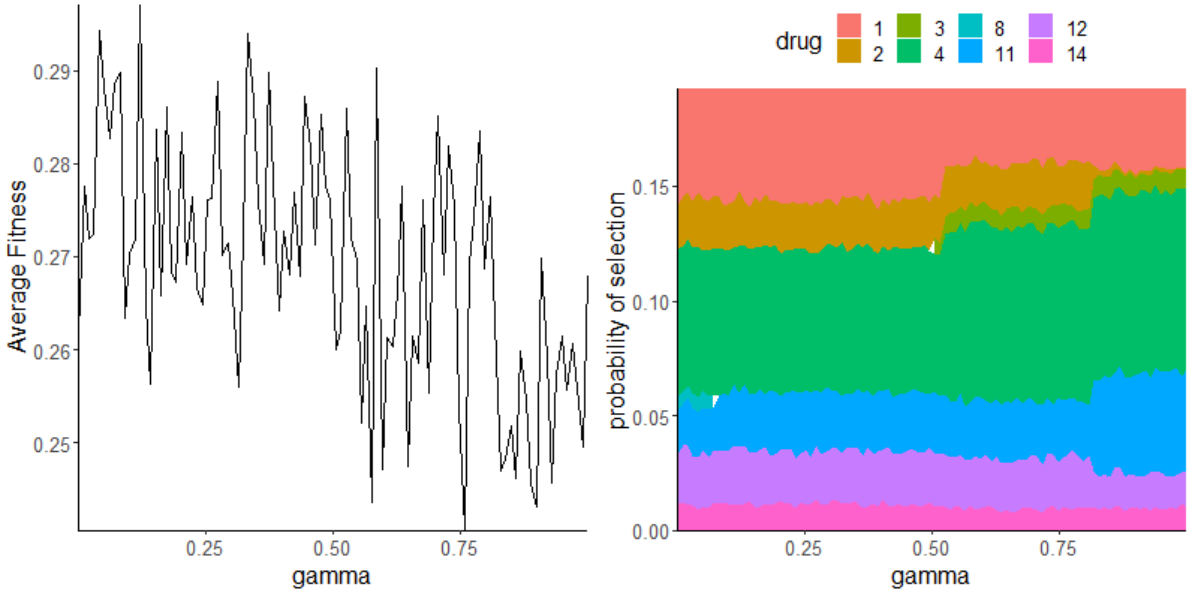

Figure S8. Effect of variation in gamma on optimal policy performance and composition

1.6 Additional Analyses

As noted in **Figure 2C** in the main text, we evaluated the performance of all A-B-A-B two-drug cycles to use as a comparison group for RL-fit and RL-genotype. In **Figure S9A**, we examine these combinations in greater depth. We also show the landscape correlation between the two drugs in every combination. We show that anti-correlated landscapes tend to make more effective combinations, likely due to collateral sensitivity. Highly correlated landscapes tend to make ineffective drug combinations, likely due to collateral resistance.

Finally, we evaluated the effect of starting population genotype on the performance of each two-drug combination. We found that the starting genotype of the population had no effect on the overall distribution of performance for these two-drug combinations (**Fig S9**).

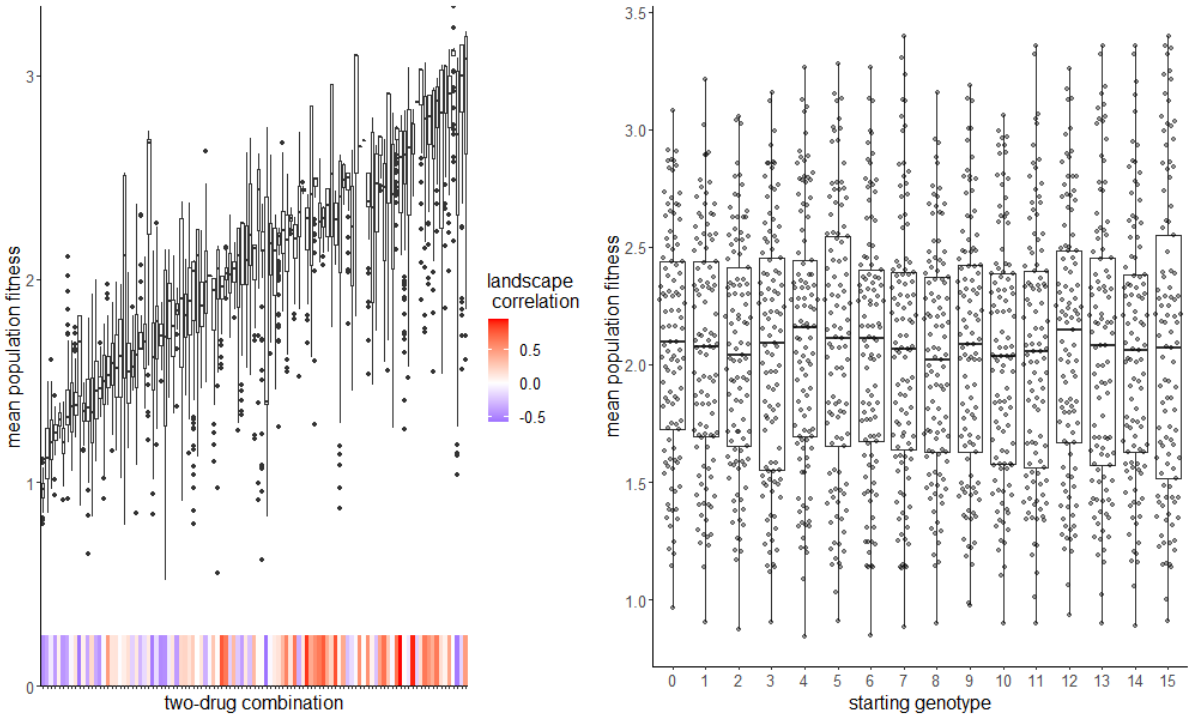

Figure S9. **Two-drug cycling policies.**